JCAMECH

Vol. 51, No. 2, December 2020, pp 486-497
DOI: 10.22059/jcamech.2020.309088.550

Mechanical behavior analysis of a clamped-clamped micro-beam with stepped viscoelastic layer under electrostatic excitation

Maryam Ghalenoei[a], Mehdi Zamanian[a,], Behnam Firouzi[a] and Seyed Ali Asghar Hosseini[a]*

[a]*Department of Mechanical Engineering, Faculty of Engineering, Kharazmi University, Mofatteh Avenue, P.O. Box 15719-14911, Tehran, Iran*

ARTICLE INFO

Article history:
Received:
Accepted:

Keywords:
MEMS
Viscoelastic
Galerkin
Assumed method
Perturbation theory

ABSTRACT

In this study, static deflection, natural frequency and nonlinear vibration in bi-layer clamped-clamped microbeam are investigated. In this configuration, the second layer is the viscoelastic layer which covers a part of the microbeam length. This model is the main element of many chemical microsensors. The governing equations of motion for the system are obtained by Lagrange method and discretized using the assumed mode method. The non-uniform micro-beam modes shape are used as the comparison function in the assumed mode method. Initially, considering the DC voltage, system static response and natural frequency around the static position are obtained. Then, considering the AC voltage, the dynamic response around the dynamic position is calculated by both analytical (perturbation method) and numerical methods (Rung-kutta) and compared for validation purposes. The effect of different geometrical parameters of the viscoelastic layer on the static and dynamic behaviors of the system is also analyzed. The results indicate that the dimensions and location of the viscoelastic layer significantly affect the static and dynamic behavior of the system. Therefore, by using this property and considering the application of microsensors, their behaviors can be made efficient. For sensors operating based on resonance frequency shift, the optimum shift of frequency state can be obtained by varying the dimensions and position of the viscoelastic layer. Moreover, time of response can be optimized when the system is operating based on changes in the capacity of a capacitor.

1. Introduction

Nowadays, the use of the electromechanical micro-sensors for measuring the mass value or the value of the pollution has received growing attention. The main element of these sensors is a clamped-clamped micro-beam which faces a fixed electrode. The DC or the combination of AC-DC voltage is applied between the micro-beam and the electrode based on the type of the application. In chemical micro-sensors, another layer named analyte is placed on the micro-beam, which is commonly from the viscoelastic material. If the applied voltage between the micro-beam and the electrode is DC, the electrostatic force deflects the micro-beam to a new position, which is called the static positions[1]. The particle absorption by the analyte layer leads to a change of static position, and so, a variation of the electric capacity between micro-beam and opposite electrode plate. This change creates an electrical current, and it is used to measure the mass of the absorbed particles. For the electrostatic voltage more than a particular value, the electrostatic force overcomes the elasticity of the micro-beam, and the micro-beam becomes unstable and attaches to the facing electrode. This voltage is called a pull-in voltage. If the applied voltage is AC-DC and the AC voltage frequency is near the natural frequency of the system, the micro-beam will resonate about the static position[2]. The resonance frequency of the system changes with the target's particle absorbed by the second layer, and this change is used as a criterion for measuring. According to the nonlinear nature of the electrostatic force, the nonlinear resonance shift is one of the undesirable phenomena in these systems. Since the performance of these sensors depends on the static and dynamic behaviors of microsystems, there is a vast body of literature on modeling and analyzing these phenomena. The most related ones are elaborated in the following.

In a study, Zhang and Zhao[3] presented a one-mode analysis method on the pull-in instability of electrostatically actuated micro-structures. They proved that the first mode is the dominant deflection shape for the beam/plate structure under electrical actuation and small axial load. The mechanical behavior of electromechanical resonator with nonlinear effects of Duffing and temperature frequency drift subjected to electrostatic actuation is

* Corresponding author. Tel.: (+98) 26345231241; e-mail: zamanian@khu.ac.ir

studied by Chen et al. [4]. They provided a model of active temperature compensation in this study. The experimental results showed that the resonator has a small duffing nonlinearity. Xu and Jia [5] studied the dynamic and static responses of a micro-cantilever under electrostatic excitation. They investigated the forced response in the system under resonant and non-resonant conditions applying perturbation theory. They also determined the parameters of the microbeam in an attempt to eliminate unfavorable dynamic properties such as jump phenomena. The dynamic behaviors of an electrostatically actuated clamped–clamped microbeam excited by two harmonic AC sources with different frequencies superimposed onto a DC voltage near the first three modes of vibrations are studied by Nizar-Jaber et al. [6]. Applying the Galerkin method, a reduced-order model is derived to simulate the static and dynamic response of the microsystem. They demonstrated that by properly tuning the frequency and amplitude of the excitation force, the frequency bandwidth of the resonator is controlled, and a good agreement between the theoretical and experimental data are reported. Pull-in instability of electrostatically actuated microcantilever is studied by Duan et al. [7] using Pull-in instability analyses for NEMS actuators with quartic shape approximation by including the effects of a fringing field and Casimir. Nonlinear dynamics of a clamped–clamped microbeam under symmetric electrostatic actuation on both sides have been investigated by Younesian et al. [8]. Primary and parametric resonances of MEMS structures based on repulsive force actuators were studied theoretically and experimentally by Zamanzadeh et al. [9]. They examined the resonance behavior of the system using a method of multiple scales perturbation theory. The mechanical behavior of an electrostatically actuated clamped-clamped microbeam under a simultaneous excitation of primary and subharmonic resonance is studied by Ilyas et al. [10] using the method of Multiple Time Scales. Uncure et al. [11] investigated the linear behavior of an electrostatically actuated clamped-clamped viscoelastic micro-beam. They considered the viscoelastic material model as the Kelvin-Voigt model. The effect of viscoelasticity on the nonlinear behavior of a shear-deformable extensible microbeam is investigated by Farokhi and ghayesh [12]. They showed that using viscoelastic instead of elastic material gives more accuracy. In another work [13], they studied the effect of the fringing field and viscoelasticity on the resonant response of an electrostatically actuated microresonators. In numerous studied the nonlinear vibration of mechanical systems were investigated [14-22]. It has been shown that depending on the value of the nonlinear electrostatic actuation, nonlinear stretching term, nonlinear curvature, and nonlinear inertia term, a softening or hardening behavior can be observed.

All of the studies mentioned above analyzed or optimized the pull-in voltage, natural frequency, static and dynamic response of a single-layer or separate microbeam. Many other works have studied the effects of adding mass [23-29] or adding a second layer on a micro-beams or micro plate [30-37]. Bouchaala et al. [23] present analytical formulations to determine the induced resonance frequency shifts of electrically actuated clamped–clamped micro and nano (Carbon nanotube) beams due to an added mass based on the Euler–Bernoulli beam theory. Analytical expressions based on perturbation techniques and a one-mode Galerkin approximation are developed to calculate the frequency shifts accurately under a DC voltage as a function of the added mass and position. The results indicated a significant increase in the frequency shift, and hence the sensitivity of detection, when scaling down to the nanoscale and using higher-order modes. They found that the perturbation technique is the most accurate method for computing the frequency shifts due to an added mass for loaded structures with DC voltage. Structural behavior of a MEMS gyroscope considering the size dependency is studied by oukad [24]. He used multiple scale perturbation techniques to study the primary resonance of the microsystem. It is shown that the tip mass dimension has a significant effect on the mechanical behavior of the MEMS gyroscope. In a study, Zamanian and et al. [25] investigated the dynamic response of a T-shaped mass attached to a clamped–clamped microbeam under electrostatic actuation with considering the stretching effect. The results showed that the nonlinear shift of the resonance frequency depends on competing between hardening stretching effect and softening electrostatic effect. Pull-in instability of multilayer micro-beams is studied by Rezazadeh et al. [30]. In this study, the nonlinear equation of motion is solved numerically using the nonlinear finite difference method. Rahmanian and Hashemi [31] studied the nonlinear behavior of bi-layer viscoelastic nano resonator under both electrostatic and piezoelectric actuation. In this study, the effect of viscoelasticity, size-dependency, and other parameters on the nonlinear behavior of the nanosystem are studied. The mechanical behavior of a microcantilever attached to a piezoelectric layer, considering bending-torsion vibrations, is examined by Mahmoudi and Jalili [32]. A size-dependent model of microcantilever under both electrostatic and piezoelectric actuation is examined by Yin et al. [33]. They derived the equation of motion applying the Hamilton principle and solved numerically by the aid of the Galerkin method and Newton downhill method. Raeesifard et al. [34] utilized five mode shapes of a uniform beam to determine the static deflection of a microcantilever with a piezoelectric layer under electrostatic actuation. They calculated the system's dynamic response by directly applying the multiple-scale method to the partial differential equation. Dufour et al. [35] studied the effect of coating viscoelastic layer on the mechanical properties of microcantilevers. They showed that the sensitivity of the cantilever increases by increasing the thickness of the coating layer. Furthermore, increasing viscoelastic thickness also culminates in an increase in the frequency noise since it leads to a decrease in the quality factor. Poloei et al. [36] examined the nonlinear dynamic behavior of the two-layered micro-cantilever that partially was covered with a Kelvin-Voigt viscoelastic layer. They used the Hamilton Principle to derive the equations and then investigated the effects of the viscoelasticity of the second layer and the shortening effect of the neutral axis on the mechanical behavior of the system. Moreover, in comparison with the previous research where the width was assumed to be fixed, the width of beam as well as cross-section are considered to be variable.

As noted in the literature review, although behavior of the microcantilever with a viscoelastic layer was evaluated in [35, 36], no studies have been performed on the static and dynamic behaviors of bi-layer clamped-clamped microbeam with viscoelastic layer. Due to the strain effect of mid-plane in the bi-layer clamped-clamped microbeam, the behavior is different from that of the microcantilever; also, due to the importance of this configuration in pollutant chemical and mass sensors, in this study, the effect of viscoelastic layer on the static deformation, natural frequency and nonlinear vibrations of bi-layer clamped-clamped microbeam is investigated. Further, by evaluating the effect of geometrical parameters and location of the viscoelastic layer, attempts are made to investigate increase in system efficiency and find the optimal configuration. Initially, considering the DC voltage, system static response and natural frequency around the static position are obtained. Then, considering the AC voltage, the dynamic response around the dynamic position is calculated by both analytical (perturbation method) and numerical methods (Rung-Kutta) and compared for validation purposes. Electrostatic sensors operate based on changes in capacitor capacity or resonance shift. When the system is operating based on the capacity change of a capacitor, natural frequency indicates sensor velocity and static deformation shows signal strength. Values of these properties depend on the location and thickness of the viscoelastic layer. In this paper, the effect of geometrical

parameters and location of viscoelastic layer is investigated while assuming constant mass or, in other words, constant volume of the viscoelastic layer. When the sensor operates based on resonant shift, nonlinear shift would be an undesirable phenomenon in the resonance frequency. In this study, the conditions, in which the system had minimum nonlinear shift, were analyzed. The results show that when the thickness of viscoelastic layer is assumed zero, it is in good conformity with previous works. The results also represent that convergence in the assumed mode method used in this paper is feasible even using a single mode, whereas in previous works and using the Galerkin method, convergence was fulfilled in the presence of 3 modes.

2. Modelling and Formulation

As shown in Fig, the considered model is a micro-beam with a thickness of t_b, which is at a distance d from the electrode. Voltage $V_{dc} + V_{ac}\cos(\Omega\hat{t})$ is applied between the micro-beam and electrode, where V_{dc}, V_{ac}, Ω, and $\hat{t}$ are DC voltage, AC voltage, AC voltage frequency, and time, respectively. The viscoelastic analyte layer that is located in the distances of l_1 and l_2 from the left end of the micro-beam is deposited on the micro-beam. The *assumed mode* method combined with the Lagrange method is used to derive the equations. To this end, the expressions of the derived kinetic energy, potential energy, and general force from the effect of *non-conservative viscoelastic* should be formed. The kinetic energy of the system is as follows:

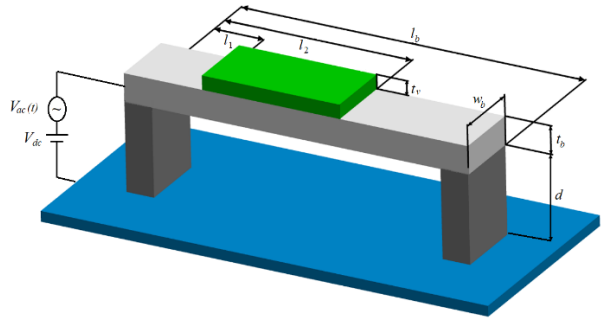

Figure1. Micro-beam layout

$$T = \frac{1}{2}\int_0^l m(\hat{x})\left(\frac{\partial \hat{w}}{\partial \hat{t}}\right)^2 d\hat{x} \tag{1}$$

where $\hat{w}$ is the displacement of the micro-beam in the transverse direction, and $m(\hat{x})$ is the mass per unit length of the micro-beam, which is defined as below:

$$\mathrm{m}(\hat{x}) = w_b\left(\rho_b t_b + \left(H_{l_1} - H_{l_2}\right)\rho_v t_v\right)$$

$$H_{l_i} = Heaviside\ function(\hat{x} - l_i) = \begin{cases} 1 & \hat{x} \geq l_i \\ 0 & \hat{x} \leq l_i \end{cases} \quad i = 1,2$$

where w_b is the width of the micro-beam and viscoelastic layer, and ρ_b and ρ_v are mass the densities of micro-beam and viscoelastic layer, respectively, and t_b and t_v are the thicknesses of the micro-beam and viscoelastic layer, respectively.

The total potential energy of the system is the sum of strain potential energy resulting from bending curvature, strain potential caused by the mid-plane stretching, and the electrical potential, which is defined as follows:

$$V = V_b + U_e - V_E \tag{3}$$

The energy of the strain potential caused by bending V_b is defined as below [36]:

$$V_b = \frac{1}{2}\int_0^l C_\eta(\hat{x})\left(\frac{\partial^2 \hat{w}}{\partial \hat{x}^2}\right)^2 d\hat{x} \tag{4}$$

where $C_\eta(\hat{x})$ is given by:

$$C_\eta(\hat{x}) = \left(1 - H_{l_1}\right)E_b I_b + \left(H_{l_1} - H_{l_2}\right)E_b \bar{I}_b + \left(H_{l_1} - H_{l_2}\right)E_v I_v + H_{l_2}E_b I_b \tag{5}$$

where the E_b and E_v are the modulus of elasticity of the micro-beam and the viscoelastic layer, respectively, and I_b is the moment of inertia of the micro-beam around the bending neutral axis in the single-layered portion. Also, $\bar{I}_b$ and I_v are the moment of inertia of the micro-beam and viscoelastic layer around the bending neutral axis and in the part of micro-beam on which the viscoelastic layer is deposited and are expressed within the following Eq.**Error! Reference source not found.** $\bar{z}_n$ is the distance of neutral axis from the center line of the micro-beam[36]:

$$I_b = \frac{w_b t_b^3}{12} \quad , \bar{I}_b = \frac{w_b t_b^3}{12} + w_b t_b \bar{z}_n^2$$

$$I_v = w_b\left(t_v \bar{z}_n^2 - (t_v^2 + t_v t_b)\bar{z}_n + \frac{1}{3}\left(t_v^3 + \frac{3}{2}t_b t_v^2 + \frac{3}{4}t_v t_b^2\right)\right)$$

$$\bar{z}_n \frac{E_v t_v (t_v + t_b)}{2(t_b E_b + t_v E_v)}$$

And the potential energy resulting from stretching effect, i.e., U_e is also defined as follow [38]:

$$U_e = \frac{1}{8l}\left[\int_0^l C_\zeta(\hat{x})\left(\frac{\partial \hat{w}}{\partial \hat{x}}\right)^2 d\hat{x}\right]^2 \tag{7}$$

where C_ζ is given by;

$$C_\zeta(\hat{x}) = \left(1 - H_{l_1}\right)E_b A_b + \left(H_{l_1} - H_{l_2}\right)E_b \bar{A}_b + \left(H_{l_1} - H_{l_2}\right)E_v A_v + H_{l_2}E_b A_b \tag{8}$$

where A_b and A_v are the cross-sections of micro-beam and viscoelastic, and $\bar{A}_b$ is the first moment of area of the micro-beam and viscoelastic layer, respectively, that are defined as follow:

$$\bar{A}_b = \frac{1}{2}w_b(t_v t_b + t_v^2 - t_v \bar{z}_n^2) \tag{9}$$

The electric potential energy is defined as follow:

(2)

$$V_E = -\frac{1}{2}\varepsilon w_b [V_{dc} + V_{ac}(t)]^2 \int_0^l \frac{1}{d - \hat{w}(\hat{x},\hat{t})} d\hat{x} \tag{10}$$

For convenience, the following set of non-dimensional parameters is introduced

$$w = \frac{-\hat{w}}{d} \quad , \quad x = \frac{\hat{x}}{l} \quad , \quad \tau = \sqrt{\frac{\rho_b t_b w_b l_b^4}{E_b I_b}} \tag{11}$$

Finally, by substituting the Eqs. **Error! Reference source not found.** , **Error! Reference source not found.**, **Error!**

Reference source not found. and **Error! Reference source not found.** into the Lagrange equation, we get:

$$L = \alpha_1 \int_0^l m(x)\left(\frac{\partial w}{\partial t}\right)^2 dx - \alpha_1 \int_0^l H_1(x)\left(\frac{\partial^2 w}{\partial x^2}\right)^2 dx - \alpha_4 \left[\int_0^l H_3(x)\left(\frac{\partial w}{\partial x}\right)^2 dx\right]^2 + \alpha_5 [V_{dc} + V_{ac}\cos(\Omega\tau)]^2 \int_{l_3}^{l_4} \frac{1}{1-w(x,t)} dx \quad (12)$$

where, parameters of α_i, $H_1(x)$, $H_3(x)$ and $m(x)$ are:

$$\alpha_1 = \frac{E_b I_b d^2}{2l_b^3} \quad , \quad \alpha_4 = \frac{w_b t_b E_b d^4}{8 l_b^3} \quad , \quad \alpha_5 = \frac{\varepsilon_0 w_b l_b}{2d} \quad (13)$$

$$H_1(x) = \left(1 - H_{l_{1/l}}\right) + \frac{\bar{I}_b}{I_b}\left(H_{l_{1/l}} - H_{l_{2/l}}\right) + \frac{E_v I_v}{E_b I_b}\left(H_{l_{1/l}} - H_{l_{2/l}}\right) + H_{l_{2/l}}$$

$$m(\mathrm{x}) = \left(1 + \left(H_{l_{1/l}} - H_{l_{2/l}}\right)\frac{\rho_v t_v}{\rho_b t_b}\right)$$

3.Reduction of order of equations by assumed mode method

In this part, the system response, i.e., W, is assumed to be $\sum_{i=1}^{M} p_i(t)\varphi_i(x)$, where $\varphi_i(x)$ is the mode shape of the non-uniform micro-beam, and $p_i(t)$ is the time coordinate response. Then, this assumed solution is substituted in the energy relation and the ODE governing equation of motion is obtained through the Lagrange equation. Hence, we must first obtain the mode shape of non-uniform micro-beam from the free vibration equation.

By substituting the linear terms of Eq. **Error! Reference source not found.** into the Lagrange equation, the linear equation governing the free vibration of the system is as follows:

$$\frac{\partial L}{\partial w} - \frac{d}{dx}\left(\frac{\partial L}{\partial_{,x}}\right) - \frac{d}{dt}\left(\frac{\partial L}{\partial_{,t}}\right) + \frac{d^2}{dx^2}\left(\frac{\partial L}{\partial w_{,xx}}\right) = 0 \quad (14)$$

$$m(x)\frac{\partial^2 w}{\partial t^2} + \frac{\partial^2}{\partial x^2}\left(H_1(x)\frac{\partial^2 w}{\partial x^2}\right) = 0$$

The answer to the Eq. (14) is supposed to be as follows:

$$w(x,t) = \varphi_n(x) e_n^{i\omega t} \quad (15)$$

where $\varphi_n(x)\ are$ the mode shapes of the non-uniform micro-beam, ω is the natural frequency of the system.
Here, $\varphi_n(x)$ consists of three parts. $\varphi_{n,1}(x)$ is mode shape function in the first part, which is a single layer $\left[0, \frac{l_1}{l}\right)$; $\varphi_{n,2}(x)$ is mode shape function in the second part, which is a double layer $\left(\frac{l_1}{l}, \frac{l_2}{l}\right)$; and $\varphi_{n,3}(x)$ is mode shape function in the third part, which is a single layer $\left(\frac{l_2}{l}, 1\right]$. So, $\varphi_n(x)$ is expressed as follows:

$$-\omega^2\varphi_{n,1}(x) + \frac{\partial^4 \varphi_{n,1}(x)}{\partial x^4} = 0 \quad , \quad 0 \le x \le \frac{l_1}{l} \quad (16)$$

$$-\left(1 + \frac{\rho_v t_v}{\rho_b t_b}\right)\omega^2\varphi_{n,2}(x) + \left(\frac{\bar{I}_b}{I_b} + \frac{E_v I_v}{E_b I_b}\right)\frac{\partial^4 \varphi_{n,2}(x)}{\partial x^4} = 0 \quad , \quad \frac{l_1}{l} \le x \le \frac{l_2}{l}$$

$$-\omega^2\varphi_{n,3}(x) + \frac{\partial^4 \varphi_{n,3}(x)}{\partial x^4} = 0 \quad , \quad \frac{l_2}{l} \le x \le l$$

The answer for each section of the differential equation will be as follows:

$$\varphi_n = \begin{cases} \varphi_{n,1}(x) = C_1\cosh(\beta_1 x) + C_2\sinh(\beta_1 x) + C_3\cos(\beta_1 \\ \varphi_{n,2}(x) = C_5\cosh(\beta_2 x) + C_6\sinh(\beta_2 x) + C_7\cos(\beta_2 \\ \varphi_{n,3}(x) = C_9\cosh(\beta_3 x) + C_{10}\sinh(\beta_3 x) + C_{11}\cos(\beta \end{cases} \quad (17)$$

where:

$$\beta_{1n} = \beta_{3n} = \sqrt{\omega_n} \quad , \quad \beta_{2n} = \left(\frac{1 + \left(\frac{\rho_v t_v}{\rho_b t_b}\right)}{\frac{\bar{I}_b}{I_b} + \frac{E_v I_v}{E_b I_b}}\omega_n^2\right)^{\frac{1}{4}} \quad (18)$$

Constant coefficients C_i are obtained from boundary conditions of clamped-clamped micro-beam for $\varphi_{n,1}(x)$ and $\varphi_{n,3}(x)$. Moreover, the following continuity conditions are obtained from equality between moment and shear force in the joining cross-section of the first part and second part and also in the joining cross-section of the second part and third part of micro-beam:

$$\varphi_{n,1}\big|_{x=0} = 0 \quad , \quad \varphi'_{n,1}\big|_{x=0} = 0 \quad , \quad \varphi_{n,3}\big|_{x=1} = 0 \quad , \quad \varphi'_{n,3}\big|_{x=1} = 0$$

$$\varphi_{n,1}\big|_{x=\frac{l_1}{l}} = \varphi_{n,2}\big|_{x=\frac{l_1}{l}} \quad , \quad \frac{\partial \varphi_{n,1}}{\partial x}\Big|_{x=\frac{l_1}{l}} = \frac{\partial \varphi_{n,2}}{\partial x}\Big|_{x=\frac{l_1}{l}}$$

$$\frac{\partial^2 \varphi_{n,1}}{\partial x^2}\Big|_{x=\frac{l_1}{l}} = \kappa_1 \frac{\partial^2 \varphi_{n,2}}{\partial x^2}\Big|_{x=\frac{l_1}{l}} \quad , \quad \frac{\partial^3 \varphi_{n,1}}{\partial x^3}\Big|_{x=\frac{l_1}{l}} = \kappa_1 \frac{\partial^3 \varphi_{n,2}}{\partial x^2}\Big|_{x=\frac{l_1}{l}} \quad (19)$$

$$\varphi_{n,2}\big|_{x=\frac{l_2}{l}} = \varphi_{n,3}\big|_{x=\frac{l_2}{l}} \quad , \quad \frac{\partial \varphi_{n,2}}{\partial x}\Big|_{x=\frac{l_2}{l}} = \frac{\partial \varphi_{n,3}}{\partial x}\Big|_{x=\frac{l_2}{l}}$$

$$\kappa_1 \frac{\partial^2 \varphi_{n,2}}{\partial x^2}\Big|_{x=\frac{l_2}{l}} = \frac{\partial^2 \varphi_{n,3}}{\partial x^2}\Big|_{x=\frac{l_2}{l}} \quad , \quad \kappa_1 \frac{\partial^3 \varphi_{n,2}}{\partial x^3}\Big|_{x=\frac{l_2}{l}} = \frac{\partial^3 \varphi_{n,3}}{\partial x^3}\Big|_{x=\frac{l_2}{l}}$$

where $\kappa_1 = \frac{\bar{I}_b}{I_b} + \frac{E_v I_v}{E_b I_b}$. By applying the above-mentioned conditions and determining the constants, the linear mode shape of the non-uniform micro-beam will be obtained:

$$\varphi_n(x) = \left(1 - H_{\frac{l_1}{l}}\right)\varphi_{n,1}(x) + \left(H_{\frac{l_1}{l}} - H_{\frac{l_2}{l}}\right)\varphi_{n,2}(x) + H_{\frac{l_2}{l}}\varphi_{n,3}(x) \tag{20}$$

By obtaining the non-uniform mode shape of the two-layered clamped-clamped micro-beam, and then by substituting the expression $\sum_{i=1}^{M} p_i(t)\varphi_i(x)$ into Eq. (20), the result will be as follows:

$$L = \alpha_1 \int_0^1 \sum_{i,j=1}^{M} m(x)\varphi_i(x)\varphi_j(x)\frac{dp_i(t)}{dt} \times \frac{dp_j(t)}{dt}dx$$

$$+ \alpha_1 \int_0^1 \sum_{i,j=1}^{M} H_1(x)p_i(t)p_j(t)\frac{d^2\varphi_i(x)}{dx^2} \times \frac{d^2\varphi_j(x)}{dx^2}dx$$

$$+ \alpha_4 \left[\int_0^1 H_3(x)p_i(t)p_j(t)\frac{d\varphi_i(x)}{d(x)} \times \frac{d\varphi_j(x)}{d(x)}dx\right]^2$$

$$- \alpha_5\big(V_{dc}$$

$$+ V_{ac}Cos(\Omega t)\big)^2 \left[\int_0^1 \sum_{i=1}^{M} p_i(t)\varphi_i(x)dx\right.$$

$$\left. + \int_0^1 \sum_{i,j=1}^{M} p_i(t)p_j(t)\varphi_i(x)\varphi_j(x)dx\right]$$

$$- \alpha_5\big(V_{dc}$$

$$+ V_{ac}Cos(\Omega t)\big)^2 \left[\int_0^1 \sum_{i,j,k=1}^{M} p_i(t)p_j(t)p_k(t)\varphi_i(x)\varphi_j(x)\varphi_k(x)\right.$$

$$- \alpha_5\big(V_{dc}$$

$$+ V_{ac}Cos(\Omega t)\big)^2 \left[\int_0^1 \sum_{i,j,k,m=1}^{M} p_i(t)p_j(t)p_k(t)p_m(t)\varphi_i(x)\varphi_j(x\right.$$

The discretized equations of motion can be obtained using the following equation:

$$\frac{\partial L}{\partial p_i(t)} - \frac{d}{dt}\left(\frac{\partial L}{\partial p_i(t)}\right) + Q_i = 0$$

where Q_i is the general force caused by non-conservative effects of viscoelastic damping and viscous damping. The virtual work resulting from the non-conservative effect of viscoelastic can be stated as follows:

$$\delta w_{n-v} = \int_V \left(H_{l_1} - H_{l_2}\right)\sigma_{n-v}\delta\varepsilon_v d_{V_v} + \int_0^1 \mu\dot{w}\delta\dot{w} \tag{23}$$
$$\sigma_{n-v} = C\dot{\varepsilon}_v$$

where d_{V_v} is the differential of the viscoelastic layer volume, C is *Kelvin-Voigt* coefficient of viscoelastic damping, μ is viscous damping coefficient and σ_{n-v} is non-conservative stress caused by the damping effect of the viscoelastic layer, and $\mathcal{E}_v$ is strain of the viscoelastic layer. In the above relations, $\mathcal{E}$ is calculated as follows [36]:

$$\varepsilon = -w''z \tag{24}$$

where, z is the distance from the bending neutral axis. It is worth mentioning that non-linear effects are neglected in the damping calculations, since the damping is small.
By substituting the above relation in the Eq. (23), we have:

$$\delta W_{nc} = \int_0^1 \mu\dot{w}\delta w + \int_{l_1}^{l_2} C_v(\dot{w}'')''\delta w \tag{25}$$
$$C_\vartheta = CI_v\left(H_{l_1} - H_{l_2}\right)$$

Now by assuming $W = \sum_{i=1}^{M} p_i(t)\varphi_i(x)$ the general forces arising from the viscoelastic layer and viscous damping will be as follows:

$$Q_i = (\alpha_7 + \alpha_6)M_5\dot{p}_i(t) \tag{26}$$

α_6 and α_7 is given by:

$$\alpha_6 = \frac{CI_v d^2}{(l_b)^4}\sqrt{\frac{E_b I_b}{\rho_b A_b}} \quad , \quad \alpha_7 = \frac{\mu d^2}{l_b}\sqrt{\frac{E_b I_b}{\rho_b A_b}} \tag{27}$$

So, by calculating all terms of Eq. (23), the motion equation is defined as follows:

$$eq_i \tag{28}$$
$$= 2\alpha_1 \int_0^1 \sum_{i=1}^{3} H_1(x)p_i(t)\left(\frac{d^2\varphi_i}{dx^2}\right)^2$$
$$+ 4\alpha_4 p_i(t)\int_0^1 \sum_{i=1}^{3} H_3(x){p_i}^2(t)\left(\frac{d\varphi_i}{dx}\right)^2$$
$$- \alpha_5(V_{dc}$$
$$+ V_{ac}\cos\Omega t)\left[\int_0^1 \sum_{i=1}^{3}\varphi_i(x) + 2\int_0^1 \sum_{i=1}^{3} p_i(t)\varphi_i(x)\right]$$
$$- \alpha_5(V_{dc}$$
$$+ V_{ac}\cos\Omega t)\left[3\int_0^1 \sum_{i=1}^{3} {p_i}^2(t){\varphi_i}^3(x)\right.$$
$$\left. + 4\int_0^1 \sum_{i=1}^{3} {p_i}^3(t){\varphi_i}^4(x)\right]$$
$$+ 2\alpha_1 \int_0^1 \sum_{i=1}^{3} m(x){\varphi_i}^2(x)\left(\frac{d^2p_i(t)}{dt^2}\right)$$
$$+ (\alpha_7 + \alpha_6)M_5\dot{p}_i(t)$$

4. Numerical Solution

If the terms including time derivatives and the terms containing V_{ac} is to be set equal to zero, in Eq. **Error! Reference source not found.**, the governing equation will become as an algebraic system. The static deflection will be obtained by solving this algebraic system as numerical and replacing the outlook into Eq. (15). In follow the function frequency response of system is

extracted for different parameters of system. Numerical results have been obtained by using Maple17 software based on the Runge–Kutta–Fehlberg method. The algorithm that finds the numerical solution using Runge-Kutta method of orders 4 and 5 is called RKF45. To solve the equation, initially, all initial conditions are set equal to zero, and the actuation frequency is considered less than the natural frequency of clamped-clamped micro-beam obtained in static solution. Then, the steady-state amplitude is obtained from time history of numerical solution. The actuation frequency is then slightly increased and the steady-state of the previous step is considered as the initial condition of the next step. At all these stages, the condition of the initial velocity has been set equal to zero. The same operation is repeated in the opposite way, i.e. the actuation frequency is considered slightly higher than the natural frequency and the initial conditions are assumed to be zero. Thus, the amplitude of the steady state is obtained from time history of the numerical solution, the actuation frequency is slightly decreased and the steady state of previous step is considered as the initial condition of the next step. The importance of these commuting solutions is that jump occurs in the forward path within the different frequency than that of backward path, and therefore, the operation is required to cover all domains.

5. Perturbation Theory

By considering one mode in Eq. **Error! Reference source not found.** , after applying the Lagrange method, the governing equation becomes as follows:

$$\begin{aligned} M_1 p_1(t) + M_2 p_1^2(t) + M_3 p_1^3(t) + M_4 + M_5 \dot{p}_1(t) \\ + M_6 \ddot{p}_1(t) + M_7 \cos(\Omega t) \\ + M_8 cos^2(\Omega t) = 0 \end{aligned} \tag{29}$$

where M_i: $i = 1..8$ is given by;

$$\begin{aligned} M_1 &= \int_0^1 \alpha_1 \left(\frac{\partial^2 \varphi}{\partial x^2}\right)^2 dx \\ &\quad - 2\alpha_5 V_{dc}^2 \int_0^1 \varphi^2 dx \\ M_2 &= -3\alpha_5 V_{dc}^2 \int_0^1 \varphi^3 dx \\ M_3 &= -4\alpha_5 V_{dc}^2 \int_0^1 \varphi^4 dx \\ M_4 &= -\alpha_5 V_{dc}^2 \int_0^1 \varphi dx \end{aligned} \qquad \begin{aligned} M_5 &= -\int_{\hat{l}_1}^{\hat{l}_2} \alpha_6 \left(\frac{\partial^2 \varphi_2}{\partial x^2}\right)^2 dx \\ &\quad - \int_0^1 \alpha_7 \varphi dx \\ M_6 &= \int_0^1 \alpha_1 \varphi^2 dx \\ M_7 &= -2\alpha_5 V_{dc} V_{ac} \int_0^1 \varphi dx \\ M_8 &= -\alpha_5 V_{ac}^2 \int_0^1 \varphi dx \end{aligned} \tag{30}$$

Assuming that nonlinear terms are of weaker order compared to linear terms, Eq. (29)can be solved with the help of multiple scales method of perturbation theory, so it Can be stated as follows:

$$\begin{aligned} p_1(t) = q_0(T_0, T_1, T_2) + \varepsilon q_1(T_0, T_1, T_2) \\ + \varepsilon^2 q_2(T_0, T_1, T_2) + \varepsilon^3 q_3(T_0, T_1, T_2) \end{aligned} \tag{31}$$

where$T_0 = t$, $T_1 = \varepsilon t$, $T_2 = \varepsilon^2 t$ are time scales, and ε the bookkeeping dimensionless parameter.
To create a balance between nonlinear, damping and actuation terms, and for the solvability of the problem and to consider all terms in the equation, the order of damping is regarded as ε^2 that is, the term with M_5 coefficient and, the order of actuation is considered ε^3 that is, the terms with M_7 and M_8 coefficients. The following equations are obtained by substituting Eq. (31) in Eq. (29), and equating the terms with same ε order:
Order(ε^0);

$$M_1 q_0 + M_2 q_0^2 + M_3 q_0^2 + M_4 = 0 \tag{32}$$

Order(ε^1);

$$M_6 D_0^2 q_1 + (M_1 + 2M_2 q_0 + 3M_3 q_0^2) q_1 = 0 \tag{33}$$

Order(ε^2);

$$\begin{aligned} M_6 D_0^2 q_2 + (M_1 + 2M_2 q_0 + 3M_3 q_0^2) q_2 \\ = -3M_3 q_1^2 q_0 - M_2 q_1^2 \\ - 2M_6 D_0 D_1 q_1 \end{aligned} \tag{34}$$

Order(ε^3);

$$\begin{aligned} M_6 D_0^2 q_3 + (M_1 + 2M_2 q_0 + 3M_3 q_0^2) q_3 \\ = -2M_6 D_0 D_1 q_2 - M_6 D_1^2 q_1 \\ - 2M_6 D_0 D_2 q_1 - 2M_2 q_1 q_2 - M_1 q_1^3 \\ - M_5 D_0 q_1 - M_7 \cos(\Omega T_0) \\ - M_8 \cos(2\Omega T_0) \end{aligned} \tag{35}$$

where $D_n = \frac{\partial}{\partial T_n}; n = 0,1,2$ and $D_n D_n = \left(\frac{\partial}{\partial T_m}\right)\left(\frac{\partial}{\partial T_n}\right)$

Assuming $\omega = \sqrt{\frac{M_1 + 2M_2 q_0 + 3M_3 q_0^2}{M_6}}$ the solution of Eq. (33) will be as follows:

$$q_1 = A(T_1, T_2) e^{i\omega T_0} + \bar{A}(T_1, T_2) e^{-i\omega T_0} \tag{36}$$

where $A(T_1, T_2)$ is a complex constant that is approached by applying the solvability conditions, so by replacing Eq. (36) into Eq. (34)

$$\begin{aligned} M_6 D_0^2 q_2 + (M_1 + 2M_2 q_0 + 3M_3 q_0^2) q_2 \\ = \left(-2i\omega M_6 \frac{\partial A}{\partial T_1}\right) e^{i\omega T_0} \\ - (M_2 + 3M_3 q_0) A^2 e^{2i\omega T_0} \\ - (2M_2 + 6M_3 q_0) A\bar{A} + C_c \end{aligned} \tag{37}$$

where C_c stands for the complex conjugate of the preceding terms. To eliminate the secular terms from Eq (37) , $\frac{\partial A}{\partial T_1}$ should be zero, consequently, $A = B(T_2)$ i.e., A is just a function of T_2 , Then, the particular solution for Eq. **Error! Reference source not found.** will be equal to:

$$\begin{aligned} q_2 = -\frac{(M_2 + 3M_3 q_0)}{3\omega^2 M_6} A^2 e^{2i\omega T_0} \\ - \frac{(M_2 + 3M_3 q_0)}{3\omega^2 M_6} \bar{A}^2 e^{-2i\omega T_0} \\ + 2\frac{(M_2 + 3M_3 q_0)}{M_6 \omega^2} A\bar{A} \end{aligned} \tag{38}$$

By substituting the Eqs. (36) and **Error! Reference source not found.** in Eq.(35) and taking into account the frequency of actuation in the form of $\Omega = \omega + \varepsilon^2 \sigma$ and maintaining the terms that create the secular term, it gets:

$$M_6 D_0^2 q_3 + (M_1 + 2M_2 q_0 + 3M_3 q_0^2) q_3 = \left[i\omega M_5 A - 2i\omega \frac{dA}{dT_2} - N_5 A^2 \bar{A} + \frac{M_7}{2} e^{i\sigma T_2} \right] e^{i\omega T_0} + C_c + NST \quad (39)$$

where σ is detuning parameter and NST stands for the rest of the terms, which do not produce secular terms.
By expressing A in the polar form ($A = \frac{1}{2} a(T_2) e^{i\beta T_2}$) and substituting it into Eq. (39), elimination of secular terms demands:

$$i\omega a' + \omega a\beta' - \frac{1}{8} N_5 a^3 + \frac{1}{2} N_3 i\omega a + \frac{F}{2} cos(\sigma T_2 - \beta) + i \frac{F}{2} sin(\sigma T_2 - \beta) = 0 \quad (40)$$

$$N_3 = \frac{M_5}{M_6} \quad ; \quad F = \frac{M_7}{M_6}$$

Assuming $\gamma = \sigma T_2 - \beta$, and separating real and imaginary parts in (40) yields

$$a' = \frac{1}{2} N_3 a + \frac{F}{2\omega} sin\gamma \quad (41)$$
$$a\gamma' = \sigma a - \frac{1}{8} N_5 a^3 + \frac{F}{2\omega} cos\gamma$$

For non-transient solution $a' = 0$, $\gamma' = 0$ so, for equilibrium solution one must set

$$\frac{1}{2} N_3 a = -\frac{F}{2\omega} sin\gamma \quad (42)$$

$$\left(\sigma - \frac{1}{8} N_5 a^2 \right) a = -\frac{F}{2\omega} cos\gamma \quad (43)$$

By squaring (42) and (43) and adding the results, the frequency response can be obtained as:

$$\frac{1}{4} N_3^2 a^2 + \left(\sigma - \frac{1}{8\omega} N_5 a^2 \right)^2 \quad (44)$$
$$a^2 = \frac{1}{4\omega^2} F^2$$

From this equation, it is obvious that the maximum amplitude occurs when terms inside the parenthesis are equal to zero. So, the maximum amplitude and resonant shift are as follows

$$a_0 = \frac{2F}{\omega N_3} \quad , \quad \sigma = \frac{N_5 a_0^2}{\omega} \quad (45)$$

The non-linear resonance frequency is obtained by substituting $\Omega = \omega + \varepsilon^2 \sigma$ in Eq (45), as follows:

$$\Omega = \omega + \frac{4 N_5 F^2}{\omega^3 N_3^2} \quad (46)$$

The term N_3 is the result of the effects of viscoelastic damping and viscous damping, which do not affect the type of hardening and softening; however, it greatly influences the vibration amplitude of the system.

6. Results:

To show the accuracy of the calculations, first, the thickness of the viscoelastic layer t_v was considered equal to zero. Next, the static deflection obtained using the assumed mode method was compared with the results of [39], which have been conducted based on the numerical shooting method. In this comparison (Figure 1), the horizontal axis is the electric voltage and the vertical axis is the dimensionless deformation of the midpoint of the micro-beam. As can be seen, the results of the present study are highly accurate. With respect to the confirmation of the results, it can be concluded that in this study, for the first time, the static solution of clamped-clamped micro-beam was obtained by the *assumed mode* method. This solution has been obtained in the previous investigations by the numerical shooting [40] and the Galerkin approach [41] method. Figure 2 shows that the method has a good convergence with a single mode, while in Galerkin's method, it occurs with at least 3 modes.
In the following, the results are presented for a micro-beam with dimensions and characteristics of $L_b = 510\mu m$, $w_b = 100\mu m$, $t_b = 1.5\mu m$, $E_b = 169e9Pa$, $\rho_b = 2330\, {kg}/{m^3}$, and $\varepsilon = 8.854e-12$, which were investigated in the previous study [40]. The specifications of the second layer are $\rho_v = 2230\, {kg}/{m^3}$, $w_v = 100\mu m$, and $E_b = 105e9Pa$. In Figure 3 and Figure 4, the effect of the change in the position second layer which covers 50% of the micro-beam length and its thickness and is equal to half of the micro-beam thickness is considered on the static deflection micro-beam and its natural frequency. As can be seen, by displacing the second layer position along the micro-beam length from the clamped side of micro-beam toward the middle part of the micro-beam, the static deflection decreases and the natural frequency increases. These changes in the middle part are more than that of other parts. So, the reinforcement of the middle section has more effect on the decrease of deflection.

Figure 3 shows that with an increase in the electrical voltage, the difference between the curves on the figure is greatly increasing. This behavior is due to the softening effects of the electrostatic actuation. The actuation force is in inverse relation to the *square* of the *distance* of the micro-beam from the opposite-electrode plate. Therefore, when the voltage increases, the curvature force increases nonlinearly and, as a result, the system with a lower degree of stiffness receives more deflection and faster pull-in voltage.

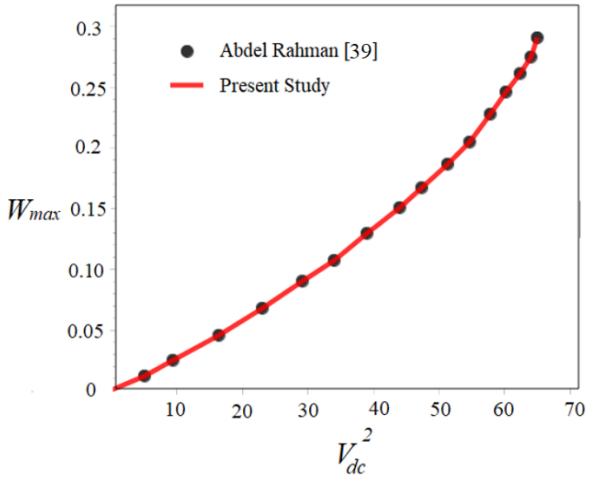

Figure 1. Variation of middle point static deflection of micro-beam with respect to the variation of DC voltage for micro-beam $l = 400mm, w_b = 45\mu m, t_2 = 2\mu m, d1\mu m$

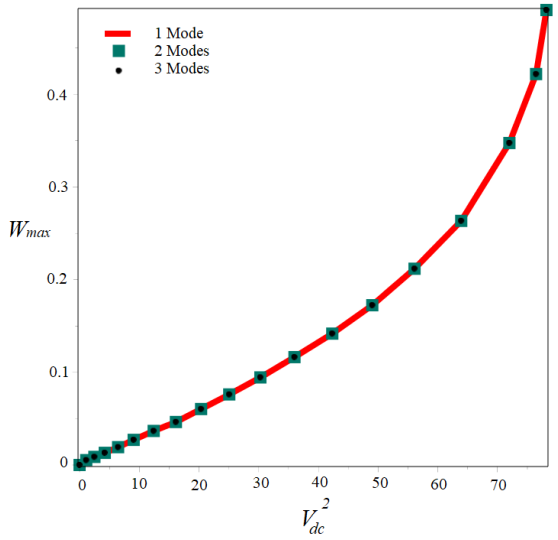

Figure 2. Middle point static deflection of micro-beam using one, two and three modes in assumed mode method.

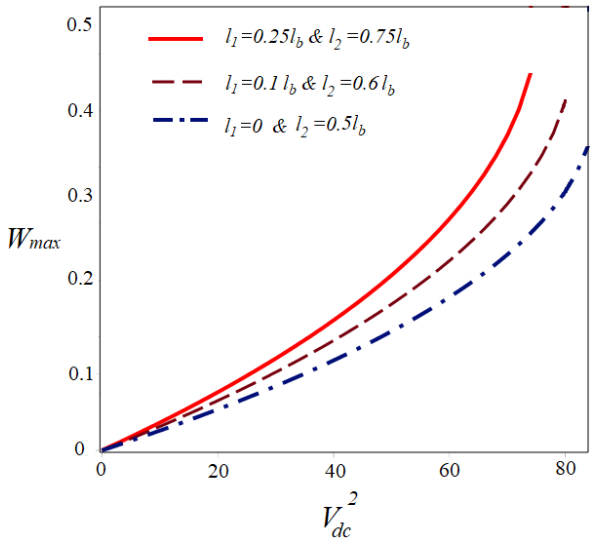

Figure 3. Variation of with respect to variation of electrostatic voltage for micro-beam with three different positions of the second layer.

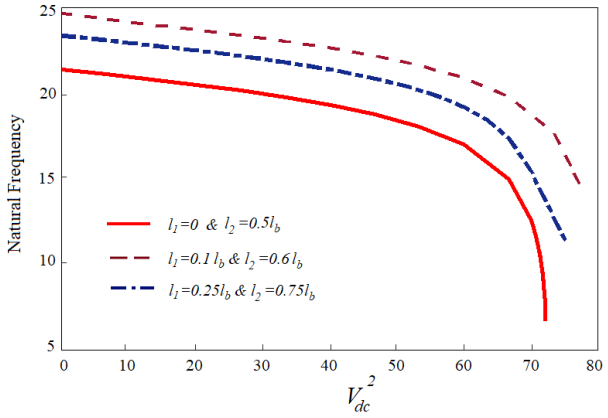

Figure 4. Variation of natural frequency with respect to electrostatic voltage for micro-beam with three different positions of the second layer.

In the following, to optimize the thickness, length, and position of the second layer, its volume is considered constant and equal to $12750\mu m^3$. It is *equivalent* to that of the second layer with a thickness of $t_v = 0.25\mu m$, which is deposited on the whole length of the micro-beam. Then, according to Figure 5, which compares system behavior within these states, the length of the second layer decreases on both ends and its thickness increases. Given that the volume is constant, only the length of the second layer is given and notating its thickness is ignored.

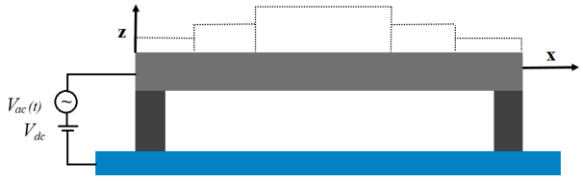

Figure 5. The second layer with a constant volume in the midpoint of the micro-beam

A comparison of static deflection for this status is presented in Figure 6. It shows that when $l_2 - l_1$ is equal to 1, then as $l_2 - l_1$ decreases to $0.5l_b$, the static deflection decreases and the pull-in voltage increases. The figure shows that this behavior is reversed by a further decrease in the second layer length.

Figure 7 shows that the same process is also true for natural frequency. These variations are confirmed like the results of Figure 3. In other words, when the second layer is located on the whole length of micro-beam, the bending stiffness of micro-beam increases by decreasing the length and increasing of the second layer thickness. Since the bending curvature in this region is higher than in other parts, it significantly affects the deformation reduction. However, with a further decrease in the length of the second layer, the layer becomes like a lumped mass in the midpoint of the micro-beam and the micro-beam acts practically as a single-layered clamped-clamped micro-beam; thus, the behavior of the system is reversed.

Based on this result, it can be inferred that if a constant volume of polymer materials is symmetrically deposited on the micro-beam, then the system has the highest natural frequency in a length and thickness approximately equal to the half-length of the micro-beam. In other words, it causes the shortest time response when designing a DC capacitive sensor.

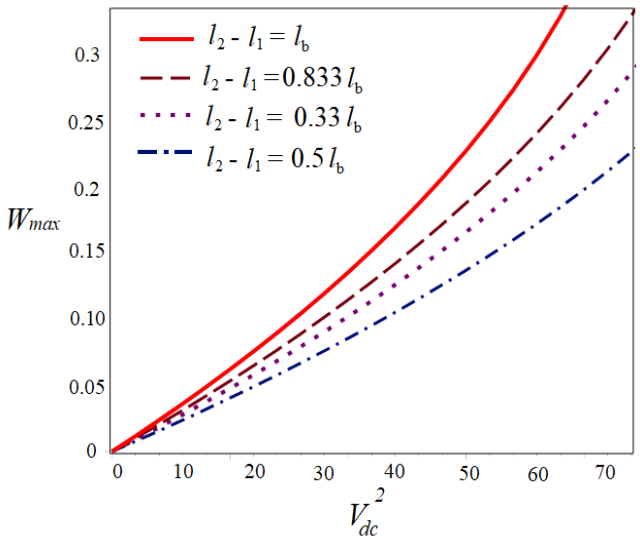

Figure 6. The static deflection by varying the voltage for the second layer with the constant volume (second layer in the midpoint of the micro-beam)

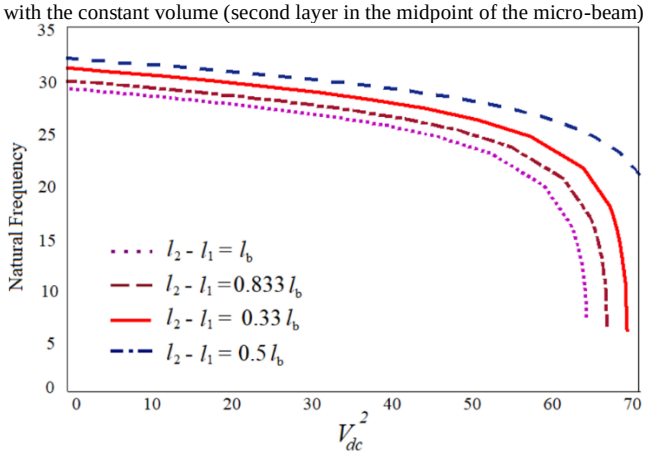

Figure 7. Natural frequency variation by varying the voltage for the second layer with the constant volume (second layer in the midpoint of the micro-beam.)

In the following, the system response under the AC-DC actuation is investigated. Eq. **Error! Reference source not found.** shows that if $F \neq 0$ and $N_5 > 0$, then the nonlinear behavior of the electrostatically-actuated micro-beam is a hardening; i.e., $\frac{\Omega}{\omega} > 1$ and $F \neq 0$ and $N_5 < 0$. Then, the behavior of the electrostatically-actuated nonlinear system is softening; i.e., $\frac{\Omega}{\omega} < 1$. In addition, this equation shows that the term N_5 is the term that is the result of the competition of the hardening effects of the middle stretching and the nonlinear softening effects of electrostatic actuation. An example of this behavior variation is shown in Figure 8, which confirms the accuracy of the obtained results.

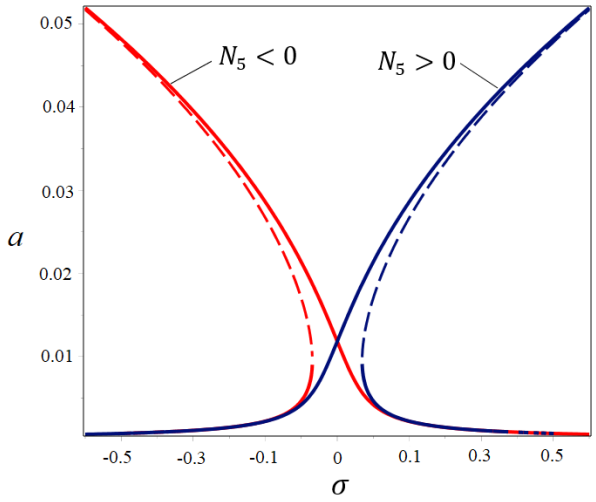

Figure 8. Effect of N_5 on frequency response curve of system.

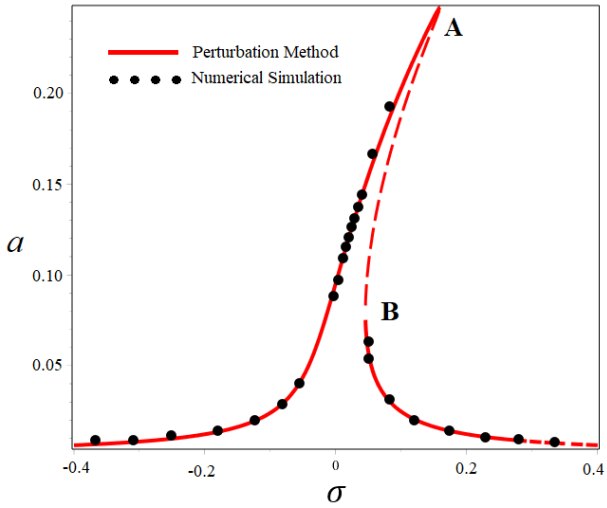

Figure 9. Comparison of Runge-Kutta method (solid circle point) and the multiple scales of Perturbation theory (solid line) for $l_1 = 0.25l_b$, $l_2 = 0.75l_b$, $\alpha^3 V_{dc}^2 = 0.61$ *and* $V_{ac} = 0.03$

Figure 9 shows that if the system has hardening behavior and the resonance frequency is considered lower than the natural frequency of the system $\sigma < \sigma_A$, then the steady-state amplitude increases with a gradual increase in the actuation frequency. Also, in A, where the difference between the actuation frequency and the natural frequency is σ_A, the amplitude jumps to the lower stable branch (Figure 10). In addition, if the resonance frequency is initially higher than the natural frequency of the system, i.e. $\sigma > \sigma_B$, then the steady-state amplitude increases with a decrease in the actuation frequency, and in σ_B the amplitude jumps to the upper branch. The same changes occur inversely for the system with the softening behavior.

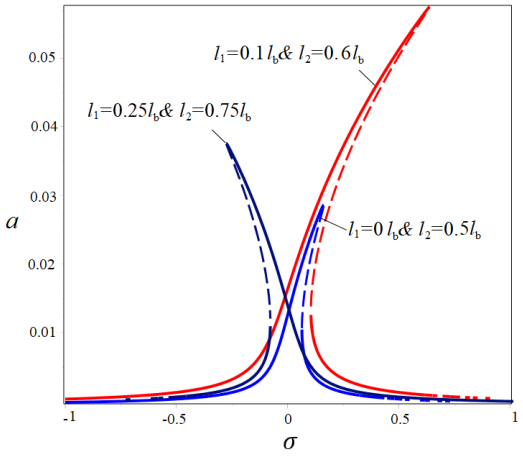

Figure 10. Vibration amplitude variation by varying the voltage for the second layer in three different positions.

Figure 10 shows the frequency response curve for the micro-beam with the viscoelastic layer deposited at a different position. As can be seen, by moving the second layer along the micro-beam length from the clamped side toward the midpoint of the micro-beam, the softening behavior approaches the linear behavior. This result is explained by the fact that reinforcement of the midpoint of the micro-beam leads to a further increase in stiffness and a decrease in the softening behavior of the system. The figure shows that in the chemical micro-sensors that operate based on resonance shift, the viscoelastic layer should preferably be deposited on the middle section of the micro-beam.

Figure 11 presents the variation of the frequency response curve in the situations in which the length of the second layer reduces and its thickness increases simultaneously. This figure shows that by decreasing the length of the second layer from l_b to $0.5l_b$, the nonlinear resonance shift decreases and the behavior of a system tends to a linear behavior. By a more decrease in the length of the micro-beam up to $0.33l_b$, the hardening behavior converts to the softening behavior and the amplitude of the steady-state vibration increases. This behavior can be explained based on Figure 6.

Overall, it can be stated that if a constant volume of material is deposited symmetrically on the micro-beam, then there is a certain thickness and length for the second layer that causes the lowest nonlinear shift of resonance frequency for micro-beam based on resonance frequency change. The results indicate that the mentioned length is almost equal to the half-length of the micro-beam.

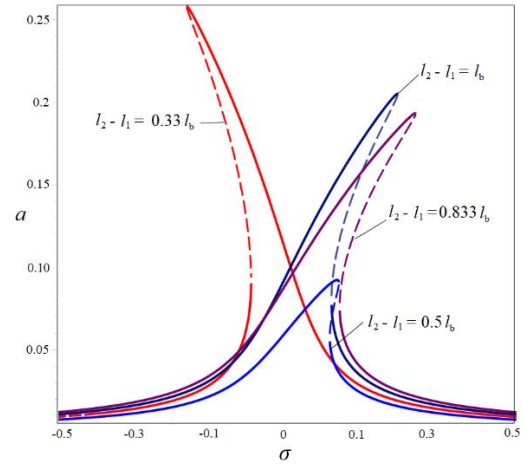

Figure 11. Vibration amplitude variations with respect to σ variations for different thicknesses of the viscoelastic layer under constant volume of the second layer.

7. Conclusion

The present study aimed to investigate static deflection, natural frequency and nonlinear vibration in bi-layer clamped-clamped microbeam. The governing equations of motion of microsystem are obtained by Lagrange method and discretized using the assumed mode method. In the assume mode method the non-uniform micro-beam modes shape are used as the comparison function. The results were obtained using analytical (perturbation) and a numerical (Rung-kutta) method; the two methods were compared to validate the obtained results. The results showed that by the change in the second layer position from the clamped side toward the middle section of the micro-beam, the static deflection decreases and the natural frequency increases. This result indicates that if a constant volume of polymer materials is symmetrically deposited on the micro-beam, the system has the highest natural frequency than the case of a length and thickness approximately equal to the half-length of the micro-beam. In other words, it causes the shortest time response when a DC capacitive sensor is designed. The results demonstrate that regarding the competition between the terms of the softening behavior of the electrostatic term and the hardening stretching term, a hardening or softening behavior for the system is observed. It is demonstrated that if the system has the softening behavior, the behavior tends to a linear system by the change of the position of the viscoelastic layer from the fixed end toward the middle side. Furthermore, we found that when the viscoelastic layer is deposited on the whole length of micro-beam, by decreasing its length symmetrically from both ends and increasing its thickness the nonlinear resonance shift, it initially decreases and then increases. The results show that the lowest nonlinear resonance shift occurs when the length of the second layer is approximately equal to the half-length of the micro-beam. Through using the results of this study, the thickness of analyte layer can be adjusted to minimize the resonance frequency shift. This minimization is very useful when the sensor is operating based on resonance shift. In addition, when the system is operating based on changes in capacitor, this modification can help optimize the system response time.

References

[1] U. Sampath, S. M. Heinrich, F. Josse, F. Lochon, I. Dufour, D. Rebiere, Study of viscoelastic effect on the frequency shift of microcantilever chemical sensors, *IEEE transactions on ultrasonics, ferroelectrics, and frequency control*, Vol. 53, No. 11, pp. 2166-2173, 2006.

[2] M. I. Younis, 2011, *MEMS linear and nonlinear statics and dynamics*, Springer Science & Business Media,

[3] Y. Zhang, Y.-p. Zhao, Numerical and analytical study on the pull-in instability of micro-structure under electrostatic loading, *Sensors and Actuators A: Physical*, Vol. 127, No. 2, pp. 366-380, 2006.

[4] D. Chen, Y. Wang, X. Chen, L. Yang, J. Xie, Temperature-frequency drift suppression via electrostatic stiffness softening in MEMS resonator with weakened duffing nonlinearity, *Applied Physics Letters*, Vol. 114, No. 2, pp. 023502, 2019.

[5] L. Xu, X. Jia, Electromechanical coupled nonlinear dynamics for microbeams, *Archive of Applied Mechanics*, Vol. 77, No. 7, pp. 485-502, 2007.

[6] N. Jaber, A. Ramini, M. I. Younis, Multifrequency excitation of a clamped–clamped microbeam: Analytical and experimental investigation, *Microsystems & nanoengineering*, Vol. 2, No. 1, pp. 1-6, 2016.

[7] J. Duan, Z. Li, J. Liu, Pull-in instability analyses for NEMS actuators with quartic shape approximation, *Applied*

Mathematics and Mechanics, Vol. 37, No. 3, pp. 303-314, 2016.

[8] D. Younesian, M. Sadri, E. Esmailzadeh, Primary and secondary resonance analyses of clamped–clamped micro-beams, *Nonlinear dynamics*, Vol. 76, No. 4, pp. 1867-1884, 2014.

[9] M. Zamanzadeh, H. M. Ouakad, S. Azizi, Theoretical and experimental investigations of the primary and parametric resonances in repulsive force based MEMS actuators, *Sensors and Actuators A: Physical*, Vol. 303, pp. 111635, 2020.

[10] S. Ilyas, F. K. Alfosail, M. I. Younis, On the application of the multiple scales method on electrostatically actuated resonators, *Journal of Computational and Nonlinear Dynamics*, Vol. 14, No. 4, 2019.

[11] M. Uncuer, B. Marinkovic, H. Koser, Simulation of clamped-free and clamped-clamped microbeams dynamics for nonlinear mechanical switch applications, in *Proceeding of*, 439.

[12] H. Farokhi, M. H. Ghayesh, Viscoelasticity effects on resonant response of a shear deformable extensible microbeam, *Nonlinear Dynamics*, Vol. 87, No. 1, pp. 391-406, 2017.

[13] H. Farokhi, M. H. Ghayesh, Electrically actuated MEMS resonators: Effects of fringing field and viscoelasticity, *Mechanical Systems and Signal Processing*, Vol. 95, pp. 345-362, 2017.

[14] Y. Zhang, Y. Liu, K. D. Murphy, Nonlinear dynamic response of beam and its application in nanomechanical resonator, *Acta Mechanica Sinica*, Vol. 28, No. 1, pp. 190-200, 2012.

[15] M. Mohammadi, M. Ghayour, A. Farajpour, Free transverse vibration analysis of circular and annular graphene sheets with various boundary conditions using the nonlocal continuum plate model, *Composites Part B: Engineering*, Vol. 45, No. 1, pp. 32-42, 2013.

[16] M. Mohammadi, M. Hosseini, M. Shishesaz, A. Hadi, A. Rastgoo, Primary and secondary resonance analysis of porous functionally graded nanobeam resting on a nonlinear foundation subjected to mechanical and electrical loads, *European Journal of Mechanics-A/Solids*, Vol. 77, pp. 103793, 2019.

[17] R. Sepahvandi, M. Zamanian, B. Firouzi, S. Hosseini, Nonlinear vibration analysis of a partially coated circular microplate under electrostatic actuationpartially coated circular microplate under electrostatic actuation, *Scientia Iranica*, Vol. 27, No. 2, pp. 715-729, 2020.

[18] M. R. Farajpour, A. Rastgoo, A. Farajpour, M. Mohammadi, Vibration of piezoelectric nanofilm-based electromechanical sensors via higher-order non-local strain gradient theory, *Micro & Nano Letters*, Vol. 11, No. 6, pp. 302-307, 2016.

[19] A. Barati, M.M. Adeli, A.. Hadi, Static torsion of bi-directional functionally graded microtube based on the couple stress theory under magnetic field, *International Journal of Applied Mechanics*, Vol. 12, No 2, pp. 2050021, 2020.

[20] M. Mohammadi, A. Rastgoo, Nonlinear vibration analysis of the viscoelastic composite nanoplate with three directionally imperfect porous FG core, *Structural Engineering and Mechanics*, Vol. 69, No. 2, pp. 131, 2019.

[21] M. Goodarzi, M. Mohammadi, A. Farajpour, M. Khooran, Investigation of the effect of pre-stressed on vibration frequency of rectangular nanoplate based on a visco-Pasternak foundation, 2014.

[22] S. Asemi, A. Farajpour, M. Mohammadi, Nonlinear vibration analysis of piezoelectric nanoelectromechanical resonators based on nonlocal elasticity theory, *Composite Structures*, Vol. 116, pp. 703-712, 2014.

[23] A. Bouchaala, A. H. Nayfeh, M. I. Younis, Analytical study of the frequency shifts of micro and nano clamped–clamped beam resonators due to an added mass, *Meccanica*, Vol. 52, No. 1-2, pp. 333-348, 2017.

[24] H. M. Ouakad, Nonlinear structural behavior of a size-dependent MEMS gyroscope assuming a non-trivial shaped proof mass, *Microsystem Technologies*, Vol. 26, No. 2, pp. 573-582, 2020.

[25] M. Zamanian, A. Karimiyan, S. Hosseini, H. Tourajizadeh, Nonlinear vibration analysis of a⊥-shaped mass attached to a clamped–clamped microbeam under electrostatic actuation, *Proceedings of the Institution of Mechanical Engineers, Part C: Journal of Mechanical Engineering Science*, Vol. 231, No. 11, pp. 2147-2158, 2017.

[26] B. Firouzi, M. Zamanian, S. Hosseini, Static and dynamic responses of a microcantilever with a T-shaped tip mass to an electrostatic actuation, *Acta Mechanica Sinica*, Vol. 32, No. 6, pp. 1104-1122, 2016.

[27] B. Firouzi, M. Zamanian, The effect of capillary and intermolecular forces on instability of the electrostatically actuated microbeam with T-shaped paddle in the presence of fringing field, *Applied Mathematical Modelling*, Vol. 71, pp. 243-268, 2019.

[28] M. Shaat, A. Abdelkefi, Modeling of mechanical resonators used for nanocrystalline materials characterization and disease diagnosis of HIVs, *Microsystem Technologies*, Vol. 22, No. 2, pp. 305-318, 2016.

[29] M. Khater, M. Al-Ghamdi, S. Park, K. M. Stewart, E. Abdel-Rahman, A. Penlidis, A. Nayfeh, A. Abdel-Aziz, M. Basha, Binary MEMS gas sensors, *Journal of Micromechanics and Microengineering*, Vol. 24, No. 6, pp. 065007, 2014.

[30] G. Rezazadeh, A comprehensive model to study nonlinear behavior of multilayered micro beam switches, *Microsystem Technologies*, Vol. 14, No. 1, pp. 135-141, 2008.

[31] S. Rahmanian, S. Hosseini-Hashemi, Size-dependent resonant response of a double-layered viscoelastic nanoresonator under electrostatic and piezoelectric actuations incorporating surface effects and Casimir regime, *International Journal of Non-Linear Mechanics*, Vol. 109, pp. 118-131, 2019.

[32] S. N. Mahmoodi, N. Jalili, Non-linear vibrations and frequency response analysis of piezoelectrically driven microcantilevers, *International Journal of Non-Linear Mechanics*, Vol. 42, No. 4, pp. 577-587, 2007.

[33] T. Yin, B. Wang, S. Zhou, M. Zhao, A size-dependent model for beam-like MEMS driven by electrostatic and piezoelectric forces: A variational approach, *Physica E: Low-dimensional Systems and Nanostructures*, Vol. 84, pp. 46-54, 2016.

[34] H. Raeisifard, M. Zamanian, M. N. Bahrami, A. Yousefi-Koma, H. R. Fard, On the nonlinear primary resonances of a piezoelectric laminated micro system under electrostatic control voltage, *Journal of Sound and Vibration*, Vol. 333, No. 21, pp. 5494-5510, 2014.

[35] I. Dufour, F. Lochon, S. M. Heinrich, F. Josse, D. Rebière, Effect of coating viscoelasticity on quality factor and limit of detection of microcantilever chemical sensors, *IEEE Sensors Journal*, Vol. 7, No. 2, pp. 230-236, 2007.

[36] E. Poloei, M. Zamanian, S. Hosseini, Nonlinear vibration analysis of an electrostatically excited micro cantilever beam coated by viscoelastic layer with the aim of finding the modified configuration, *Structural Engineering and Mechanics*, Vol. 61, No. 2, pp. 193-207, 2017.

[37] M. Zamanian, S. Javadi, B. Firouzi, S. Hosseini, Modeling and analysis of power harvesting by a piezoelectric layer coated on an electrostatically actuated microcantilever, *Materials Research Express*, Vol. 5, No. 12, pp. 125502, 2018.

[38] A. F. Marques, R. C. Castelló, A. Shkel, Modelling the electrostatic actuation of MEMS: state of the art 2005, 2005.

[39] E. M. Abdel-Rahman, M. I. Younis, A. H. Nayfeh, Characterization of the mechanical behavior of an electrically actuated microbeam, *Journal of Micromechanics and Microengineering*, Vol. 12, No. 6, pp. 759, 2002.

[40] M. I. Younis, A. Nayfeh, A study of the nonlinear response of a resonant microbeam to an electric actuation, *Nonlinear Dynamics*, Vol. 31, No. 1, pp. 91-117, 2003.

[41] A. H. Nayfeh, M. I. Younis, A new approach to the modeling and simulation of flexible microstructures under the effect of squeeze-film damping, *Journal of Micromechanics and Microengineering*, Vol. 14, No. 2, pp. 170, 2003.